FOURTEENTH EUROPEAN ROTORCRAFT FORUM

Paper No. 61

AEROELASTIC RESPONSE CHARACTERISTICS OF A ROTOR EXECUTING ARBITRARY HARMONIC BLADE PITCH VARIATIONS

TOMOARI NAGASHIMA, GIZO HASEGAWA
TOSHIFUMI NEKOHASHI and TAKEICHIRYO HIROSE

DEPARTMENT OF AERONAUTICAL ENGINEERING
THE NATIONAL DEFENSE ACADEMY
YOKOSUKA, JAPAN

20-23 September, 1988
MILANO, ITALY

ASSOCIAZIONE INDUSTRIE AEROSPAZIALI
ASSOCIAZIONE ITALIANA DI AERONAUTICA ED ASTRONAUTICA

AEROELASTIC RESPONSE CHARACTERISTICS OF A ROTOR EXECUTING ARBITRARY HARMONIC BLADE PITCH VARIATIONS

Tomoari Nagashima, Gizo Hasegawa, Toshifumi Nekohashi
and Takeichiryo Hirose
Department of Aeronautical Engineering
The National Defense Academy
Yokosuka, Japan

Abstract

As a basic research for an active vibration control using high frequency blade pitch oscillations, analytical and experimental studies to explore aeroelastic characteristics of the collective control responses of a rotor due to the harmonic blade pitch variations, with the hub fixed in space, are carried out. The steady state responses of dynamic hub vertical load are analyzed by modal integral methods using the Loewy's two dimensional unsteady airfoil theory for a rotor in hover, while in forward flight, the Miller's three dimensional one is utilized. To verify the computed results, force tests to measure the hub vertical loads over a wide frequency range up to fifth harmonics of the rotor speed are conducted with a one-bladed model rotor. Flow visualization studies are also made for a rotor in hover to disclose diversity of the wake geometries piled beneath the rotor under various pitch change frequency ratios. Both numerical and experimental results reveal their unique dependencies on the pitch change frequency as well as the modal parameters and for a rotor in forward flight, there may be the optimum blade pitch variations by which the hub dynamic vertical load could be minimized.

1. Introduction

Vibration is a problem of long standing in helicopter engineering. Considerable progress have been made over the years in vibration control technology, still vibrations remain to be troublesome and difficult problems to deal with.

Reichert in Ref. 1 and Loewy in Ref. 2 discussed various vibration reduction devices and methods for a helicopter and stressed a need to establish the practical hub load prediction methods with improved accuracy.

On the other hand, in accordance with rapid progress in computer technology as well as modern control theory, a new vibration supression method utilizing the active control technology receives increasing attention.[3][4]

The higher harmonic control (H.H.C.) is a typical approach along this concept and its usefulness as a practical vibration control system have been demonstrated theoretically and experimentally by the wind tunnel tests on the model rotor[5] as well as flight tests on the actual machines.[6]

It is well recognized that the active vibration control has an advantage of significant weight saving to be coupled with the structural optimization.[7] From design point of view, eliminating rotor induced dynamic hub loads at the rotor itself seems to be the most promising and reasonable concept.

Nevertheless, because of its sophisticated nature, the physical reasons why such an active control system as the H.H.C. could reduce the vibration level so effectively and what are the key factors to govern dynamic control responses of a rotor undergoing such high frequency blade pitch variations have not yet been made clear.

This will be attributed to the lack of knowledges concerning the aeroelastic behaviour of hub dynamic load induced by a rotor. In addition, little experimental data is available for the verifications of theoretical results.

In this research, as a basic study for the active vibration control utilizing high frequency blade pitch oscillations, the steady state responses of the hub vertical load due to harmonic blade pitch variations are investigated analytically and experimentally, both for a rotor in hover and in forward flight with emphasis placing on their aeroelastic behaviour.

The responses of the hub vertical load due to harmonic blade pitch variations are selected as a simple but typical collective control response of a rotor executing arbitrary pitch change motions, with the hub fixed in space.

The hub loads responses due to hub motions are referred to as the rotor impedances. In this regard, this study will be considered as a companion research to those given by K. Kato et al. in Ref. 7. The steady state responses of a flexible blade forced by sinusoidal blade pitch variations with arbitrary frequency are determined by the linear modal equations of motion. The generalized unsteady aerodynamic loads are computed based on the Loewy's two dimensional unsteady airfoil theory[8] for a rotor in hover, while in forward flight, the Miller's three dimensional theory[9] is utilized with modifications being made so as to be able to apply the theory to any rotor undergoing arbitrary frequency blade pitch variations, independent from harmonics of the rotor speed.

Using these responses, together with unsteady aerodynamic loads which are composed of the circulatory and noncirculatory lifts, the frequency responses of the hub vertical load are obtained for a rotor in hover.

In forward flight, the harmonic balance method is used to solve the modal equations of motion of a blade and unsteady aerodynamic equations simultaneously. The effects of sinusoidal blade pitch application on their steady state responses are numerically analyzed, because in this case, they will become a function not only of the rotor speed and its harmonics but also blade pitch change frequency.

Numerical results obtained for various flight conditions show that there may exist the optimum blade pitch variations by which the steady state responses of the hub vertical load could be minimuzed.

To verify the accuracies of computed results, experimental studies for a rotor in hover and forward flight are conducted with a one-bladed rotor. Dynamic force tests are planned intentionally to measure the hub vertical load over a wide frequency range up to fifth harmonics of the rotor speed. Measured data are fed into a F.F.T. processor to obtain their averaged amplitudes and phases spectra.

Flow visualization studies for a rotor in hover are also made using a smoke injection method. Pictures obtained show clearly the facts that the frequency responses of the hub vertical load are closely related to the wake geometries being piled beneath the rotor.

The purpose of this research is to develop the methods, which can be able to predict precisely influences of unsteady aerodynamic forces on the hub vertical load responses, by taking the returning wake into consideration. In the following sections, discussions are made mainly on their frequency responses in hover with introducing computed and measured results for the steady state responses in forward flight subsidiary.

2. Aeroelastic Response Characteristics of a Rotor in Hover Executing Arbitrary Harmonic Blade Pitch Variations

2.1 Derivation of equations of motion and basic assumptions

A linear modal analysis method to predict steady state aeroelastic responses of the hub vertical load for a hovering rotor due to sinusoidal blade pitch variations with arbitrary frequency, with the hub being fixed in space is described.

The equations of equilibrium for the coupled flap bending and torsion of a blade excited by mechanically as well as aeroelastically in hover are derived by the Lagrange method based on the engineering beam theory, together with the Loewy's two dimensional unsteady airfoil theory.

The following assumptions are made.

(1) The rotor is a single-bladed one being cantilevered to the hub at an offset of e from the axis of rotation. At the blade root, there is no built-in twist nor precone angle.
(2) The hub is fixed in space.
(3) The blade is composed of an isotropic and homogeneous materials.
(4) The blade cross section is structurally symmetrical about the major principal axis and has two distinct points, center of gravity (C.G.) and center of elasticity (C.E.).
(5) Both the elastic and the C.G. axes are assumed to be straight and in parallel with each other along the blade span. The offset distance between them is e_g, positive when the elastic axis lies in the rearward.

(6) The blade can be deformed in flapwise bending normal to elastic axis and torsion around it. The inplane bending is neglected for simplicity, although the method used can be readily extended to treat the fully coupled blade dynamics.
(7) During deformations, the cross sections normal to the elastic axis remain unchanged.
(8) The blade pitch angle is varied about the feathering axis which is considered to be coincident with the C.G. axis. The blade pitch implementation is described as $\Theta = \Theta_0 + \Delta\Theta$, where Θ_0 is the collective pitch and $\Delta\Theta$ is the sinusoidal excitation with an arbitrary frequency ω, respectively.
(9) There is no mechanical δ_3 coupling and dynamic interactions between control system flexibilities and blade torsional deformation are neglected.
(10) The section aerodynamic loads are computed by using the Loewy's unsteady two dimensional thin airfoil theory and integration is made in the blade element theory fashion.
(11) In constructing the two dimensional wake model, the vertical spacing of returning shed vortices for a successive rotor revolution is assumed to be constant and be able to define simply by the average inflow velocity as a function of the static thrust for a given collective pitch.
(12) Stall and compressibility are neglected.

The coordinate systems used for describing the blade motions are shown in Fig. 1.

Brief description of them are given below.

X_I, Y_I, Z_I system is the inertial system with the origin at hub center. The blade rotates with X_R, Y_R, Z_R system which is the one when X_I, Y_I, Z_I system rotates about the Z_I axis by $\psi = \Omega t$, Ω is the rotational speed of the rotor and assumed to be constant. The X_R axis is coincident with the blade C.G. axis, while the Y_R axis is pointing toward the leading edge in the hub plane. X_E, Y_E, Z_E system is the moving system obtained when X_R, Y_R, Z_R system rotates about the X_R axis by Θ, then move the origin along the major principal axis by e_g so as to coincide the X_R axis with the undeformed elastic axis.

The blade deformation processes referred to the X_E, Y_E, Z_E system are defined by following sequences. A point P on the undeformed elastic axis undergoes translational deformation u, v = 0, w in the X_E, Y_E, Z_E directions, respectively and occupies the position P' on the deformed elastic axis.

The angular positions of the cross section containing P' relative to X_R, Y_R, Z_R system is given by the three Euler angles $(\Theta+\phi, -w', v'=0)$, where $(\,)'$ denotes $\partial(\,)/\partial X_E$ and Θ and ϕ are the geometrical pitch angle and torsional deformation, respectively. ξ, η, ζ system is the local orthogonal system attached to the deformed blade such that the ξ axis is tangential to the deformed elastic axis and the η and ζ axes are the major and minor principal axes of the cross section. X_A, Y_A, Z_A system is also the local one obtained by setting $\Theta + \phi \equiv 0$ in ξ, η, ζ system, so the Y_A axis remains parallel to the hub plane. This system is used for the evaluation of aerodynamic loads.

After fairly cumbersome calculations to evaluate the Lagrangian function, the following coupled equations of equilibrium will be obtained as

$$(EI_1 w'')'' - (Tw')' - (Te_g\phi')' + m(\ddot{w} + e_g\ddot{\phi}) = L \tag{1}$$

$$-\{(Tk_A^2 + GJ)\phi'\}' - (Te_g w)' + m\Omega^2(k_{m1}^2 - e_g^2)\phi$$

$$+ mk_m^2\ddot{\phi} + me_g\ddot{w} = M - m(k_m^2 - e_g^2)(\ddot{\theta} + \Omega^2\theta) \tag{2}$$

where

$$T \cong \Omega^2 \int_r^R m(r + e)dr$$

and $(\dot{})$ denotes the differentiation with respect to time.

Structural properties appeared in Equs. (1) and (2) are EI_1: bending stiffness about the η axis, GJ: torsional stiffness, m: mass per unit blade length, km: mass radius of gyration of blade cross section, $k_m = \sqrt{k_{m1}^2 + k_{m2}^2} \cong k_{m1}$, k_{m2}: principal radii of gyration of blade cross section, k_A: polar radius of gyration of blade cross section, respectively.

In deriving Equs. (1) and (2), additional assumption is made for the cross sectional integral, that is the offset distance between the elastic and tension axes, e_A which is defined by $e_A = \int_A \eta dA/A$, is equal to e_g, $e_g = \int_A \rho\eta dA/m$ where ρ and A are the blade mass density and the cross sectional area, respectively. The motion of equilibrium given by Equs. (1) and (2) are reduced to those of Nagaraja and Pierce in Ref. 10 by putting $e_A = 0$ and eliminating the terms connected with θ.

L and M in the right hand sides of Equs. (1) and (2) denote the section lift and pitching moment, respectively. At present, a great variety of numerical methods to predict the aerodynamic loads in hover are available, however, L and M are computed by the Loewy's theory in this study, by virtue of its ability to capture unsteady effects due to the returning shed wake analytically.

Expanding w and ϕ with the coupled natural mode shapes as

$$w = \Sigma W_j q_j \tag{4}$$

$$\phi = \Sigma \Phi_j q_j \tag{5}$$

where W_j, Φ_j and q_j denote the jth coupled natural mode shapes and the jth generalized coordinates, respectively.

Substitute Equ. (4) into Equs. (1) and (2), and then discretize the spatial dependence of the equations of equilibrium using the orthogonality property with respect to jth natural mode shapes given by

$$\int_0^R m[W_j W_\ell + e_g(\Phi_j W_\ell + \Phi_\ell W_j) + k_m^2 \Phi_j \Phi_\ell]dX_E$$

$$= \begin{cases} M_\ell & \text{for } \ell = j \\ 0 & \text{for } \ell \neq j \end{cases} \qquad (\ell, j = 1, 2, \ldots, N) \tag{6}$$

We can read the modal equations of motion which govern the aeroelastic responses for the jth generalized coordinates as follows

$$M_j\ddot{q}_j + M_j(1 + ig_j)\nu_j^2 q_j = \int_0^R [LW_j + M\Phi_j - m(k_m^2 - e_g^2)(\ddot{\Theta} + \Omega^2\Theta)\Phi_j]dX_E \qquad (j = 1, 2, \ldots, N) \qquad (7)$$

where g_j and ν_j are the structural damping and the natural frequency for the coupled jth natural mode shapes, respectively.

The natural mode shapes and their natural frequencies can be determined numerically as the solutions of linear, coupled homogeneous differential equations which are gained by letting L, M and Θ in Equs. (1) and (2) to be zero with the appropriate boundary conditions.

2.2 Aeroelastic response characteristics of hub vertical load in hover due to harmonic blade pitch variations

As can be seen in Ref. 8, Loewy's two dimensional theory represents the motions of a rigid airfoil section in terms of pitching α and heaving h motions, both of which are referred to the feathering axis located at a distance of ab after from the mid chord.

Within a linear theory, we can express h, α by a linear combination of the elastic deformations w, ϕ as follows.

$$h = -(w + e_g\phi) \quad , \quad \alpha = \Theta + \phi. \qquad (8)$$

Using relations given by Equ. (8), we can obtain unsteady section lift L and pitching moment M in Equ. (7) as functions of elastic deformations of the blade as well as the harmonic pitch variations.

$$L = a_0\rho_a r\Omega bC'(k, n, d)\{r\Omega(\phi + \Delta\Theta) - (\dot{w} + e_g\dot{\phi}) + b(\dot{\phi} + \Delta\dot{\Theta})(\tfrac{1}{2} - a)\} + \rho_a\pi b^2\{r\Omega(\dot{\phi} + \Delta\dot{\Theta}) - (\ddot{w} + e_g\ddot{\phi}) - ab(\ddot{\phi} + \Delta\ddot{\Theta})\} \qquad (9)$$

$$M = \rho_a\pi b^3[(a - e_g)(\ddot{w} + e_g\ddot{\phi}) - r\Omega(\tfrac{1}{2} + a - e_g)(\dot{\phi} + \Delta\dot{\Theta}) - b\{\tfrac{1}{8} + (a - e_g)^2\}(\ddot{\phi} + \Delta\ddot{\Theta})] + a_0\rho_a b^2 r\Omega(a - e_g - \tfrac{1}{2})C'(k, n, d)\{(\dot{w} + e_g\dot{\phi}) - r\Omega(\phi + \Delta\Theta) - b(\tfrac{1}{2} - a)(\dot{\phi} + \Delta\dot{\Theta})\} \qquad (10)$$

where a_0, ρ_a, b and a are section lift curve slope, density of air, blade semichord and distance between the mid chord and the feathering axis, positive aft., respectively.

It should be noted that in Equs. (9) and (10), the circulatory lift and moment due to the collective pitch, Θ_0 are omitted as they are considered to be the time invariant component defining the trim states

about which the dynamic deformations could occur. C' (k, n, d) is the Loewy's modified lift deficiency function. For a single bladed rotor, C' is defined as the function of three nondimensional parameters, k, n, d, which are given respectively by

$$k = \frac{b\omega}{r\Omega} \ , \ n = \frac{\omega}{\Omega} \ , \ d = \frac{2\pi u}{b\Omega} \tag{11}$$

where d denotes the wake spacing for a two dimensional wake model. The wake spacing is assumed to be constant for the rotor with a given collective pitch Θ_0, and can be defined by the average inflow velocity u.

Let us define the harmonic blade pitch excitation, $\Delta\Theta$ as $\Delta\Theta = \hat{\Theta}e^{i\omega t}$ and assume the steady state responses of the jth generalized coordinates to be

$$q_j = \hat{q}_j e^{i\omega t} \qquad (j = 1, 2, \ldots, N) \tag{12}$$

then the complex amplitudes $\hat{q}_j$ can be gained in a matrix form as

$$[H]\{\hat{q}\} = \{S\}\hat{\Theta} \ , \ \{\hat{q}\} = [H]^{-1}\{S\}\hat{\Theta} \tag{13}$$

$$[H] = \begin{bmatrix} -\omega^2(M_1-A_{11})-i\omega B_{11} & \cdots & \omega^2 A_{1j}-i\omega B_{1j} & \cdots & \omega^2 A_{1N}-i\omega B_{1N} \\ +M_1\nu_1^2(1+ig_1)-C_{11} & \cdots & -C_{1j} & \cdots & -C_{1N} \\ \vdots & & \vdots & & \vdots \\ \omega^2 A_{j1}-i\omega B_{j1} & \cdots & -\omega^2(M_j-A_{jj})-i\omega B_{jj} & \cdots & \omega^2 A_{jN}-i\omega B_{jN} \\ -C_{j1} & \cdots & +M_j\nu_j^2(1+ig_j)-C_{jj} & \cdots & -C_{jN} \\ \vdots & & \vdots & & \vdots \\ \omega^2 A_{N1}-i\omega B_{N1} & \cdots & \omega^2 A_{Nj}-i\omega B_{Nj} & \cdots & -\omega^2(M_N-A_{NN})-i\omega B_{NN} \\ -C_{N1} & \cdots & -C_{Nj} & \cdots & +M_N\nu_N^2(1+ig_N)-C_{NN} \end{bmatrix} \tag{14}$$

$$\{S\} = \begin{Bmatrix} \omega^2 D_1+i\omega E_1+F_1 \\ \vdots \\ \omega^2 D_j+i\omega E_j+F_j \\ \vdots \\ \omega^2 D_N+i\omega E_N+F_N \end{Bmatrix} \tag{15}$$

$$\{\hat{q}\} = \begin{Bmatrix} \hat{q}_1 \\ \vdots \\ \hat{q}_j \\ \vdots \\ \hat{q}_N \end{Bmatrix} \tag{16}$$

$A_{j\ell}$, $B_{j\ell}$, $C_{j\ell}$ (j, ℓ = 1, 2, ..., N) and D_j, E_j, F_j (j = 1, 2, ..., N) in Equs. (14) and (15) denote the jℓth elements of the squire matrices [A], [B], [C] and the jth components of the vectors {D}, {E}, {F},

given by the following modal integral, respectively.

$$A_{j\ell} = \int_0^R \pi\rho_a b^2 \Big| (-W_\ell - e_g\Phi_\ell - ab\Phi_\ell)W_j + b[(a - \bar{e}_g)(W_\ell + e_g\Phi_\ell) - b\{\frac{1}{8} + (a - \bar{e}_g)^2\}\Phi_\ell]\Phi_j \Big| dX_E$$

$$B_{j\ell} = \int_0^R \rho_a Vb \Big| [a_0 C'(k,n,d)\{-W_\ell - e_g\Phi_\ell + b(\frac{1}{2} - a)\Phi_\ell\} + \pi b\Phi_\ell]W_j + [-\pi b^2(\frac{1}{2} + a - \bar{e}_g)\Phi_\ell + a_0 b(-a + \bar{e}_g + \frac{1}{2})C'(k,n,d)\{-W_\ell - e_g\Phi_\ell + b(\frac{1}{2} - a)\Phi_\ell\}]\Phi_j \Big| dX_E$$

$$C_{j\ell} = \int_0^R a_0\rho_a V^2 bC'(k,n,d)\Phi_\ell\{W_j + b(-a + \bar{e}_g + \frac{1}{2})\Phi_j\}dX_E$$

$$D_j = \int_0^R \pi\rho_a b^3 \Big| aW_j + [b\{\frac{1}{8} + (a - \bar{e}_g)^2\} + m(k_m^2 - e_g^2)]\Phi_j \Big| dX_E$$

$$E_j = \int_0^R \rho_a Vb^2[\{a_0(\frac{1}{2} - a)C'(k,n,d) + \pi\}W_j + \{a_0 b(-a + \bar{e}_g + \frac{1}{2}) \times C'(k,n,d)(\frac{1}{2} - a) - \pi b(\frac{1}{2} + a - \bar{e}_g)\Phi_j]dX_E$$

$$F_j = \int_0^R [a_0\rho_a V^2 bC'(k,n,d)W_j + \{a_0\rho_a V^2 b^2(-a + \bar{e}_g + \frac{1}{2})C'(k,n,d) - m(k_m^2 - e_g^2)\Omega^2\}\Phi_j]dX_E$$

$$(j, \ell = 1, 2, \ldots, N)$$

where $\bar{e}_g$ is nondimensioned e_g by b, $\bar{e}_g = e_g/b$.

It is understood that the amplitude and phase responses of the rotating blade due to the harmonic pitch excitation defined by Equs. (13), (14) and (15), are largely dependent upon not only the modal parameters, W_j, Φ_j, ν_j and g_j but also the frequency ratio, n as well as the collective pitch angle, θ_0 through the modified lift deficiency function $C'(k,n,d)$, thus indicating the importance to take the returning shed wake into account for the wake modeling.

When $\hat{q}_\ell$ ($\ell = 1, 2, \ldots, N$) are determined from Equ. (13), the blade elastic deformation along the C.G. axis can be written as

$$w_{C.G.} = w + e_g\phi = \sum_{\ell=1}^{N}(W_\ell + e_g\Phi_\ell)\sum_{j=1}^{N}\left[[H]^{-1}\{S\}\right]_{j\ell}\hat{\theta}e^{i\omega t} \qquad (17)$$

Because the dynamic hub vertical load, T can be obtained as the total summation of the distributed inertial loads due to blade elastic deformats given by Equ. (17) and the unsteady section lift by Equ. (9), the steady state responses of the hub vertical load per unit harmonic blade pitch excitation can be defined as

$$\frac{T}{\hat{\theta}} = \sum_{\ell=1}^{N}\omega^2\int_0^R[m(W_\ell + e_g\Phi_\ell)\sum_{j=1}^{N}\left[[H]^{-1}\{S\}\right]_{j\ell}dX_E + \frac{1}{\hat{\theta}}\int_0^R L dX_E \qquad (18)$$

3. Experimental Studies

The apparatus at the low speed wind tunnel test section is shown in Fig. 2. The wind tunnel testings are conducted with a one-bladed rotor arrangement so that the wake geometries and their induced effects may be simplified.

The blade is a hollow, wooden spar and rib structure with laminated F.R.P. skin. The planform is a rectangular with a radius of 850mm and a constant chord of 100mm. The cross section is NACA 0014 and there is no precone and pretwist angles. With respect to the cross sectional properties, both the C.G. and elastic axes are almost straight, however, they are separated each other with a offset distance of 30mm. The typical mass and elastic properties of the blade are listed in Table 1. The first four natural mode shapes and frequencies, which are computed for Ω = 360 R.P.M. and $\theta_0 = 0°$ by the finite element method are shown in Fig. 3.

The apparatus is equipped with two different kinds of d.c. motors, one to drive the rotor and the other for the blade pitch control, so as to realize arbitrary blade pitch excitations over a wide range of normalized frequency. The blade pitch angle is forced to vary sinuisoidally around the feathering axis which is coincident with the C.G. axis. The applied blade pitch variations around the collective pitch angle are measured by a potentiometer. The hub vertical loads are measured by strain gages banded on both surfaces of the thin phospherous bronze plate (0.3mm thick) which is designated to able to detect the dynamic loads acting on the blade not as the moments but the total reaction shear forces acting at the integrated hub flexure flame. Measured hub loads as well as blade pitch motions are picked up through a slip ring and after amplified, they are fed into a two channel F.F.T. processor to obtain their amplitude and phase spectra.

Force tests for a rotor in hover are made at the constant rotor speed of 360 R.P.M. for five different collective pitch settings ($\theta_0 = 0°, 3°, 6°, 9°, 12°$), with varying blade pitch exciting frequency by a increment of 1 Hz, while the hub vertical loads are measured at every frequency ranging from 2 Hz to 30 Hz, the fifth harmonics of the rotor speed.

For a rotor in forward flight, measurements are made at four different tip speed ratios, μ from 0.1 to 0.4 with the collective pitch being fixed to $\theta_0 = 6°$. In this case, sinusoidal blade pitch variations are applied with arbitrary combinations of the amplitude, frequency and phase angle, however, efforts are concentrated to the hub load measurement at rather narrow frequency ranges close to the integer multiples of the rotor speed. The reduced frequency at the 75% radius corresponding to the test conditions cover a range of $0.02 \sim 0.41$ and typical Reynolds number is 10^5 at the 75% radius for Ω = 360 R.P.M. The section lift curve slope of the blade is deduced to be $a_0 = 4.27$ from the static hover tests which will be used in numerical analyses instead of the theoretical one, 2π.

The flow visualizations using a smoke of evaporating kerosine are also made with another one-bladed model rotor with a radius of 800mm and

a chord of 55mm. The blade is made of solid plywood and has a hollow groove through which a smoke is guided to the blade tip. A smoke is injected into the air through the special smoke injection unit utilizing leading edge separation vortex of a delta wing, by which a smoke could be confined within the core structures of the tip vortices and long term tip vortices behaviour would be observed.

4. Comparisons between Numerical and Experimental Results

4.1 Frequency responses of the hub vertical load for a rotor in hover

Typical examples of data reductions by an F.F.T. processor are shown in Fig. 4. These are the three dimensional displays of the amplitude spectra for the applied blade pitch motions (Fig. 4.a) and the hub vertical loads (Fig. 4.b) for $\theta_0 = 0°$, respectively. It is observed that reliable input and output relations can be realized over the frequency range to be concerned.

Comparisons between computed and measured frequency responses of the hub vertical load for a rotor in hover are shown in Fig. 5 for $\theta_0 = 0°$ and in Fig. 6 for $\theta_0 = 6°$. The top and bottom figures in Fig. 5 and Fig. 6 are the nondimensioned amplitude and phase spectra for steady state responses of the hub vertical load, respectively.

The computed results depicted in these figures are obtained by approximating the blade elastic deformations with the first two natural mode shapes (Fig. 3). The exclusion of the torsion dominated modes (3rd mode) is justified because their natural frequencies are fully separated from the frequency range to be tested. The modal damping coefficients (Table 1) which are obtained for the stationary blade using an experimental modal analysis are introduced into numerical analyses.

By observing Fig. 5 and Fig. 6, the contributions of unsteady aerodynamic forces due to the returning shed wake and inertia forces due to the blade elastic deformations on the dynamic hub load responses are clearly understood. Significant features of them are (1) conspicuous amplitude decrease and rapid phase shift near the integer multiples of the rotor speed, (2) marked amplitude increase due to the resonance at the first natural frequency (3) alleviation of the returning wake effects with increasing collective pitch angles. The computed results based on the Loewy's two dimensional rigid wake model show quite well agreement with experimental ones and the importance to include the returning wake effects for the accurate hub dynamic loads prediction is ascertained.

4.2 Wake visualizations

Pictures obtained by the wake visualization for a rotor in hover whose blade pitch angle varied sinusoidally with arbitrary frequency are shown in Fig. 7. Test conditions are fixed to $\Omega = 150$ R.P.M., $\theta_0 = 6°$ and five different normalized frequencies of $n = 0, 0.5, 1.0, 1.5$ and 2.0. The pitch control amplitude is set to $3.5°$.

Fig. 7.1 gives a wake geometry for n = 0, that is, for rotor in static hover condition where the tip vortex trajectory up to seven revolutions of the rotor can be clearly recognized. Pictures for integer n are shown in Fig. 7.2 (n = 1) and Fig. 7.3 (n = 2), while for non-integer n, those are shown in Fig. 7.4 (n = 0.5) and Fig. 7.5 (n = 1.5), separately.

The behaviour of tip vortices and their spacial arrangements are quite different depending on whether blade pitch change frequency is a integer multiples of the rotor speed or not. When normalized frequency, n is non-integer, the tip vortices system show remarkable instabilities due to their nonlinear interactions and regular and stable wakes cannot be observed. It is not difficult to suppose that such unique dependencies of the hub vertical load responses on the normalized frequency as those depicted in Fig. 5 and Fig. 6 must be heavily related to their wake dynamics and structures, several of which are declared by pictures shown in Fig. 7.

4.3 Steady state responses in forward flight

As a typical example of numerical analysis for a rotor in forward flight, computed results for steady state responses of the hub vertical load at $\mu = 0.3$ are introduced in Fig. 8 ∿ Fig. 11. These are obtained based on the Miller's three dimensional unsteady theory with a semi-rigid wake model.

In this case, in contract with a rotor in hover, the phase angles of applied pitch variations play a critical role for hub vertical load responses. Hereafter, the blade pitch variations are defined by $\theta = \theta_0 + \hat{\theta} \sin(n\psi - \phi)$, where $\hat{\theta}$, n, ψ and ϕ are the pitch change amplitude, normalized frequency, blade azimuth angle and phase angle, respectively and effects of n and ϕ on the hub vertical load responses are predicted numerically with setting $\theta_0 = 6°$ and $\hat{\theta} = 3°$.

The measured and computed results for n = 0 are shown in Fig. 8. Upper two figures labelled (a) and (b) are the measured and computed time histories with the abscissas being time in sec and the blade azimuth angle in degrees, respectively, while lower two (c) and (d) are their F.F.T. results where the abscissas are the frequency in Hz. It should be noted that the abscissas in (a) are scaled to about 60% of those in (b). Owing to the fact that there is no blade pitch excitation for n = 0, frequency contents in the time histories are only limited to the rotational speed of rotor and its harmonics.

The computed and measured results for n = 1 are presented in Fig. 9 with the control phase angle, ϕ being fixed to 191°. This phase angle of 191° is selected as one at which the computed hub vertical load amplitude can be minimized under a given operating conditions. By comparing Fig. 9 with Fig. 8, it is reasonably anticipated that for a rotor in forward flight, the hub vertical load responses could be remarkably reduced by a proper application of the harmonic blade pitch variations.

To clarify the effects of a discrepancy between the blade pitch variation frequency and that of rotor on the hub vertical load responses,

computed and measured time histories and their spectra for two different non-integer normalized frequencies are shown in Fig. 10 (n = 0.9) and Fig. 11 (n = 1.1). Distinctive features to be identified in the hub load responses for non-integer normalized frequencies are the beating phenomena in their time histories which, in turn are resulted in the spectra with frequency contents not only at the rotor speed, its harmonics and the pitch control frequency but also the sum and substraction frequencies between them.

Generally speaking, it may be said safely that the computed results based on the Miller's three dimensional unsteady theory give fairly well predictions for the hub vertical load responses due to the harmonic blade pitch variations with arbitrary frequency, however, the most important finding in this study is that a slight discrepancy between the pitch control frequency and that of rotor as well as an ill suited control phase angle may bring undesirable large increase in the hub vertical load responses.

5. Conclusions

Basic analytical and experimental researches to explore the aeroelastic behaviour of the hub vertical load due to the harmonic blade pitch variations with arbitrary frequency are conducted. Analytical model to predict the steady state responses of the hub vertical load are developed using the Loewy's two dimensional unsteady airfoil theory for a rotor in hover and the Miller's three dimensional one for in forward flight.

To verify the theoretical results, force tests in hover and forward flight and wake visualization studies in hover with a one-bladed rotor are carried out. Comparisons between measured and computed results show quite well coincidence and validity and usefulness of the proposed hub load prediction method are substantiated.

It is clearly understood that the wake dynamics and structures play an essential role for aeroelastic behaviour of the hub loads responses. For a rotor in yaw, there may exist the optimum blade pitch variations which could be minimized the hub vertical load responses.

References

1. G. Reichert: "Helicopter Vibration Control-A Survey", Vertica, Vol. 5, No. 1, 1981.

2. R. G. Loewy: Helicopter Vibrations; A Technological Perspective, Journal of A.H.S., Vol. 29, No. 4, 1984.

3. J. A. Molusis, C. E. Hamond and J. H. Cline: A Unified Approach to the Optimum Design of Adaptive and Gain Scheduled Controllers to Achieve Minimum Helicopter Rotor Vibration, Journal of A.H.S., Vol. 28, No. 2, 1983.

4. M. K. Davis: Development and Evaluation of a Generic Active Helicopter Vibration Controller, 1984 Lichten Award Paper, 10th E.R.F., 1984.

5. F. J. McHugh and J. Shaw, Jr.: Benefits of Higher Harmonic Blade Pitch; Vibration Reduction, Blade-Load Reduction and Performance Improvement, A.H.S. Mideast Region Symposium on Rotor Technology, 1976.

6. F. K. Straub and E. V. Byrns, Jr.: Application of Higher Harmonic Blade Feathering on the OH-6A Helicopter for Vibration Reduction, NASA CR 4031, 1986.

7. K. Kato et al: Experimental Substantiation for Hovering Rotor Vertical Impedance Calculations, J.A.S., Vol. 18, No. 6, 1981.

8. R. G. Loewy: A Two Dimensional Approximation to The Unsteady Aerodynamics of Rotary Wings, J.A.S., Vol. 24, No. 2, 1957.

9. R. H. Miller: Rotor Blade Harmonic Air Loading, AIAA Journal, Vol. 2, No. 7, 1964.

10. K. S. Nagaraja and G. A. Pierce: Aeroelastic Response Characteristics of Rotor Blade, AIAA Paper 0699, 1980.

Table 1 Mass and elastic properties

Blade radius	$R = 0.85m$
Blade chord	$2b = 0.1m$
Offset between feathering axis and elastic axis Offset between C.G. axis and elastic axis	$e_f = 0.03m$ $e_g = -0.03m$
Blade cross-section moments of inertia about elastic axis	$I_1 = 4.21 \times 10^{-7} m^4$ $I_2 = 4.71 \times 10^{-9} m^4$
Mass of blade	$m = 2.57 \times 10^{-2} Kg$
Blade moment of inertia about elastic axis	$I_{EA} = 5.15 \times 10^{-5} Kgm^2$
Bending stiffness	$EI_2 = 40.96 Nm^2$
Torsional stiffness	$GJ = 42.14 Nm^2/rad$
Structural damping coefficient in the jth vibration mode	$g_1 = g_2 = 0.025$, $g_3 = 0.06$

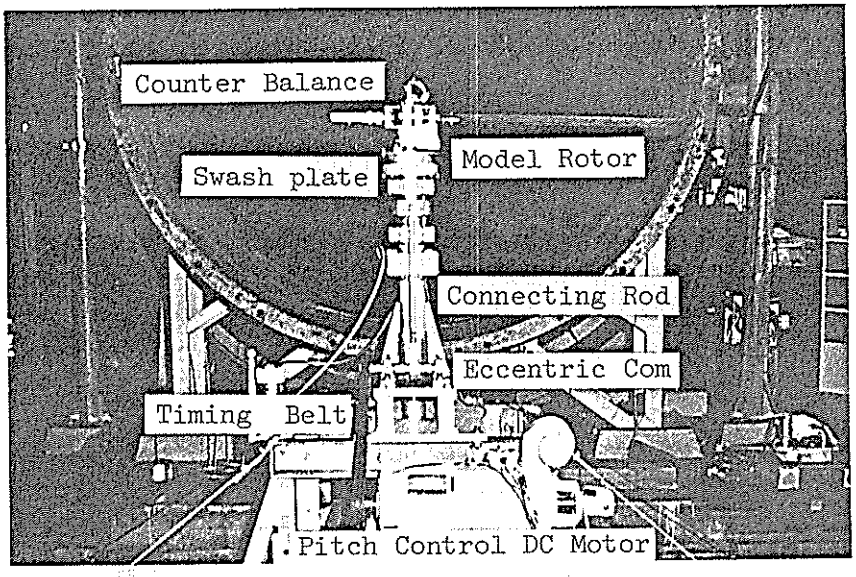

Fig.1 Experimental apparatus

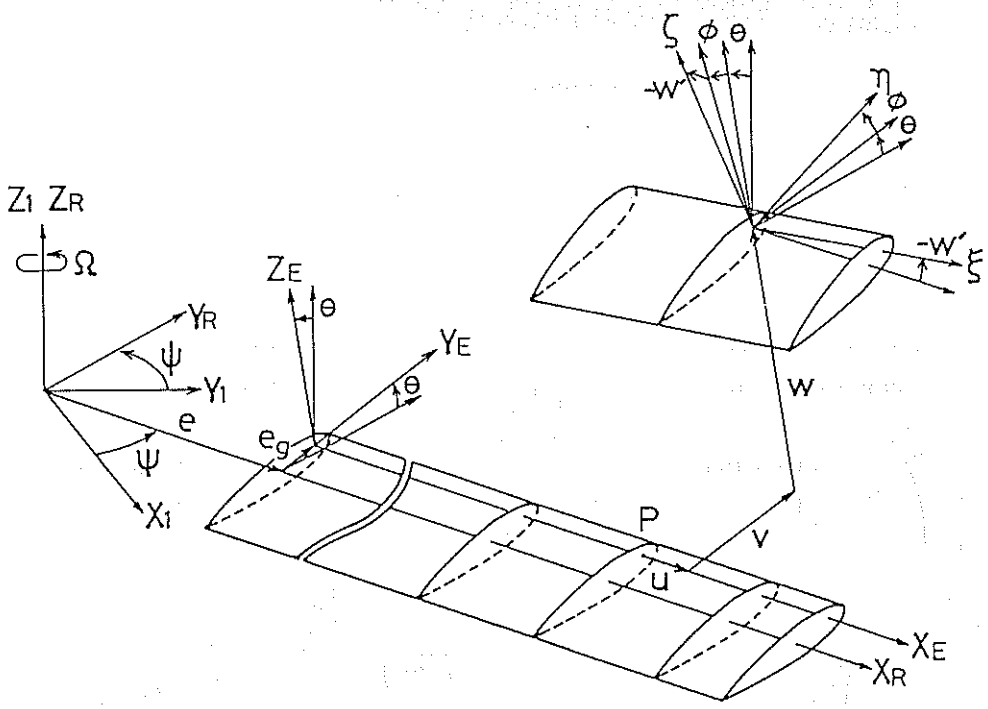

Fig.2 Coordinate systems

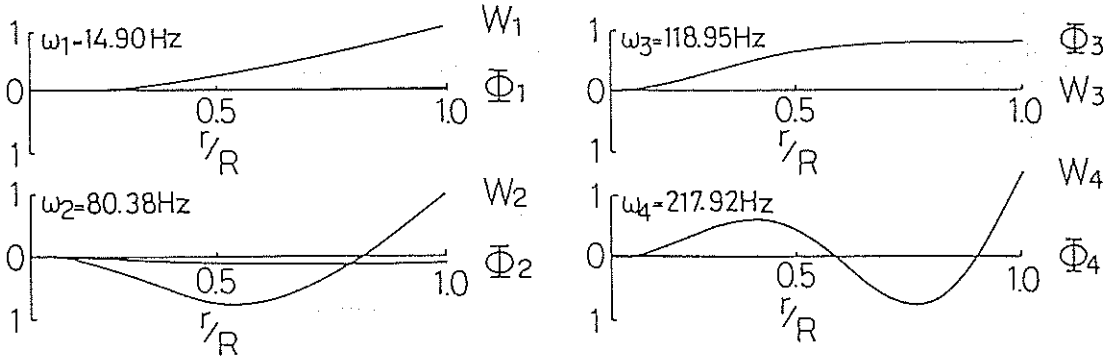

Fig.3 Vibration characteristics of blade

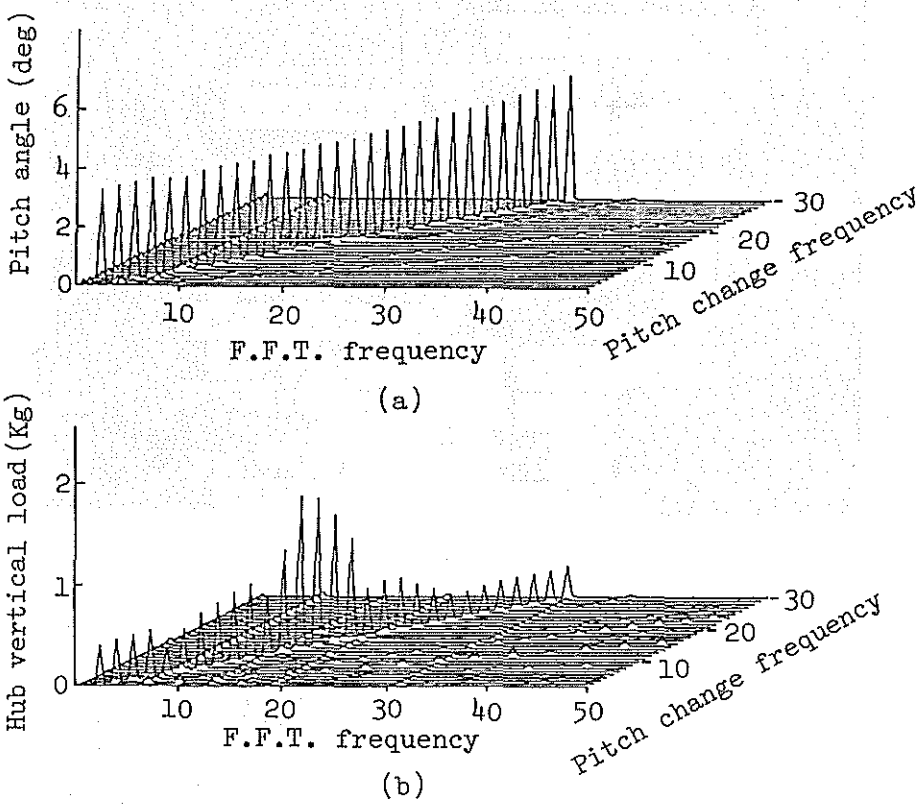

Fig.4 F.F.T. results for blade motion(a) and hub vertical loads(b)

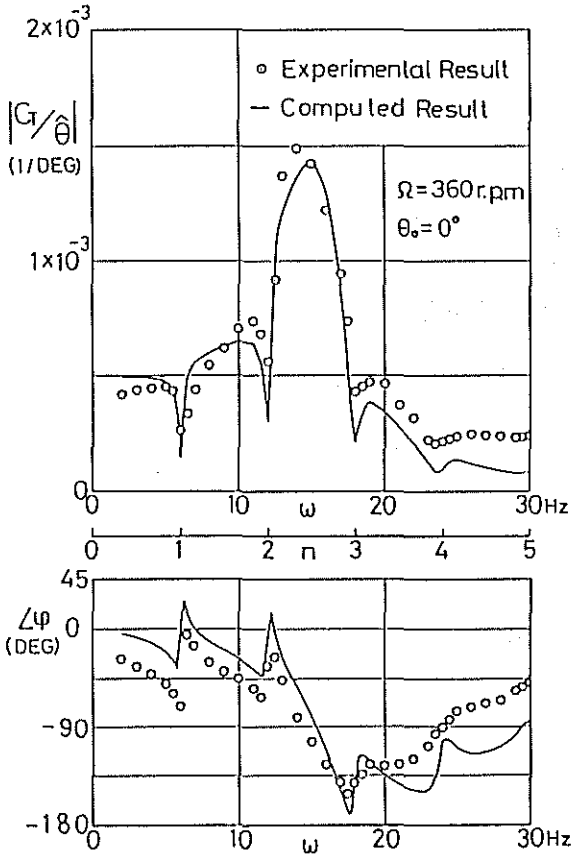

Fig.5 Frequency response of hub vertical load $\theta_0 = 0°$

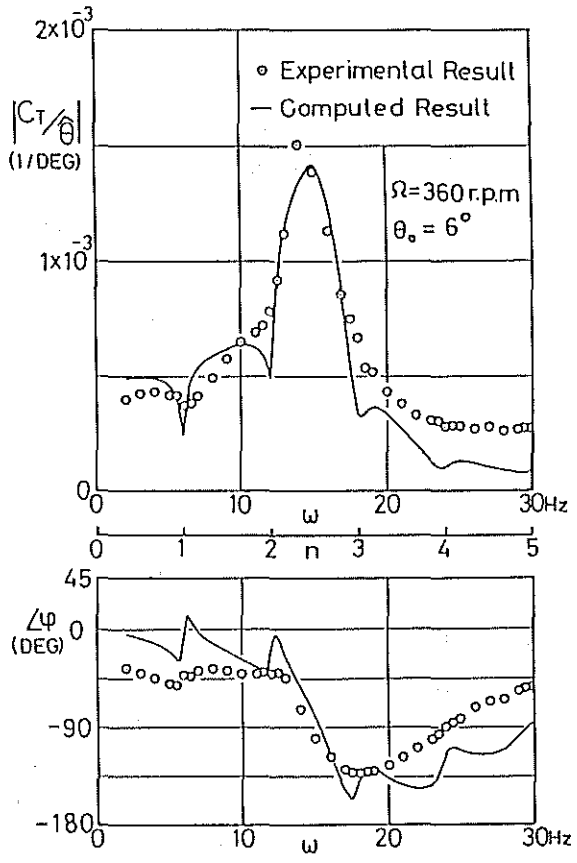

Fig.6 Frequency response of hub vertical load $\theta_0 = 6°$

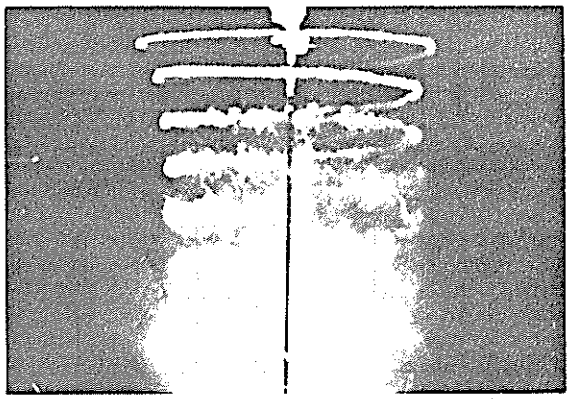

Fig.7.1 Tip vortex geometry (n=0)

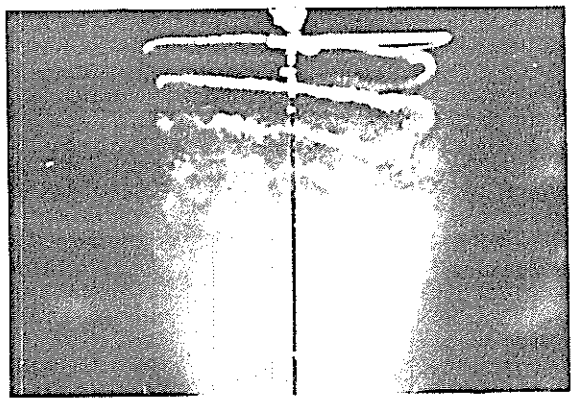

Fig.7.2 Tip vortex geometry (n=1)

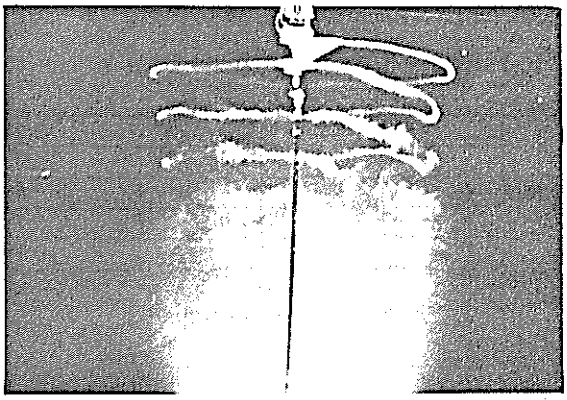

Fig.7.3 Tip vortex geometry (n=2)

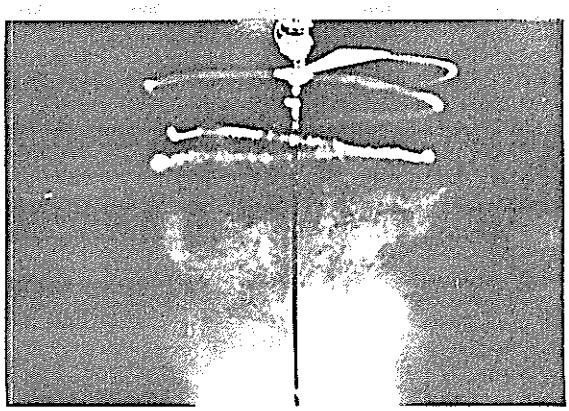

Fig.7.4 Tip vortex geometry(n=0.5)

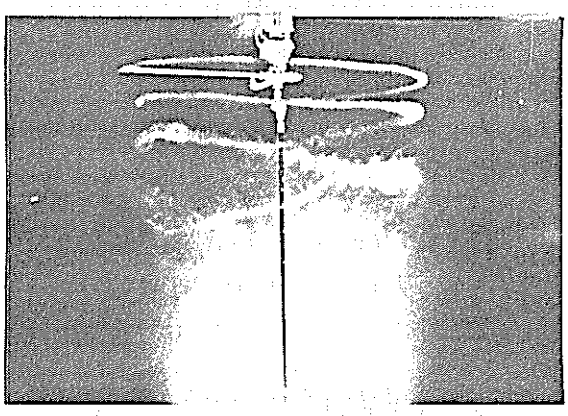

Fig.7.5 Tip vortex geometry (n=1.5)

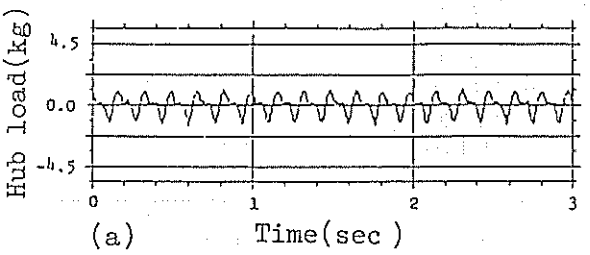

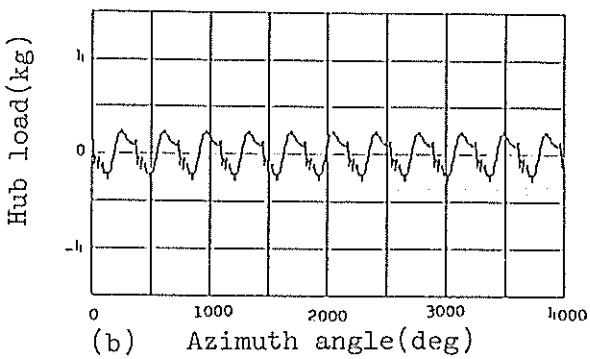

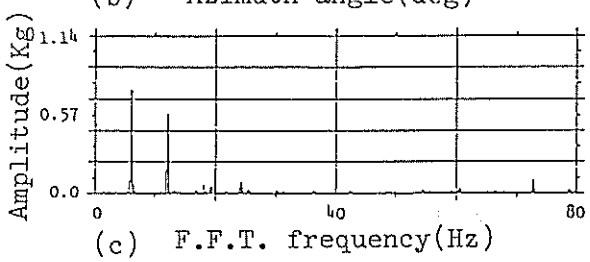

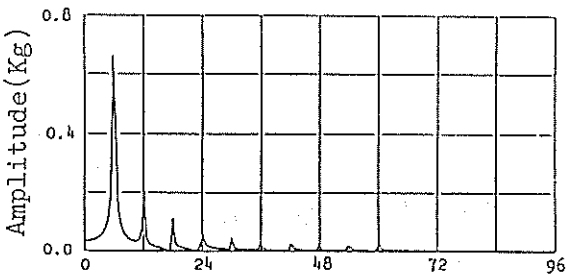

Fig.8 Time histories and their F.F.T. results (n=0)

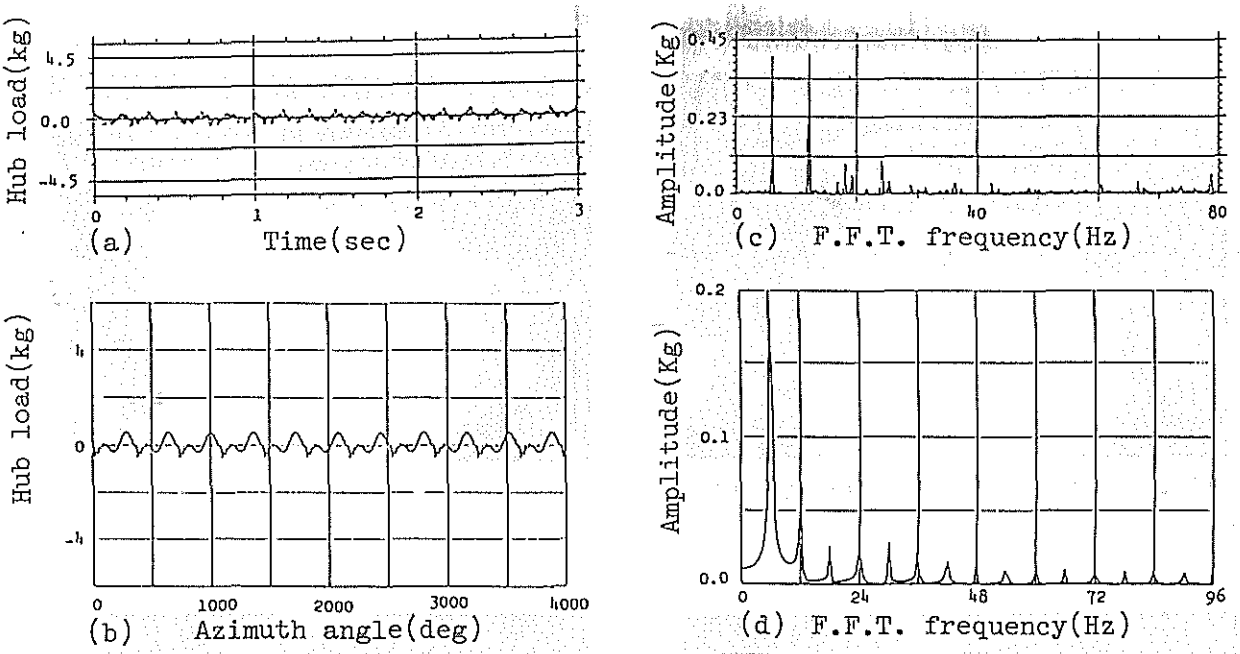

Fig.9 Time histories and their F.F.T. results (n=1,ϕ=191°)

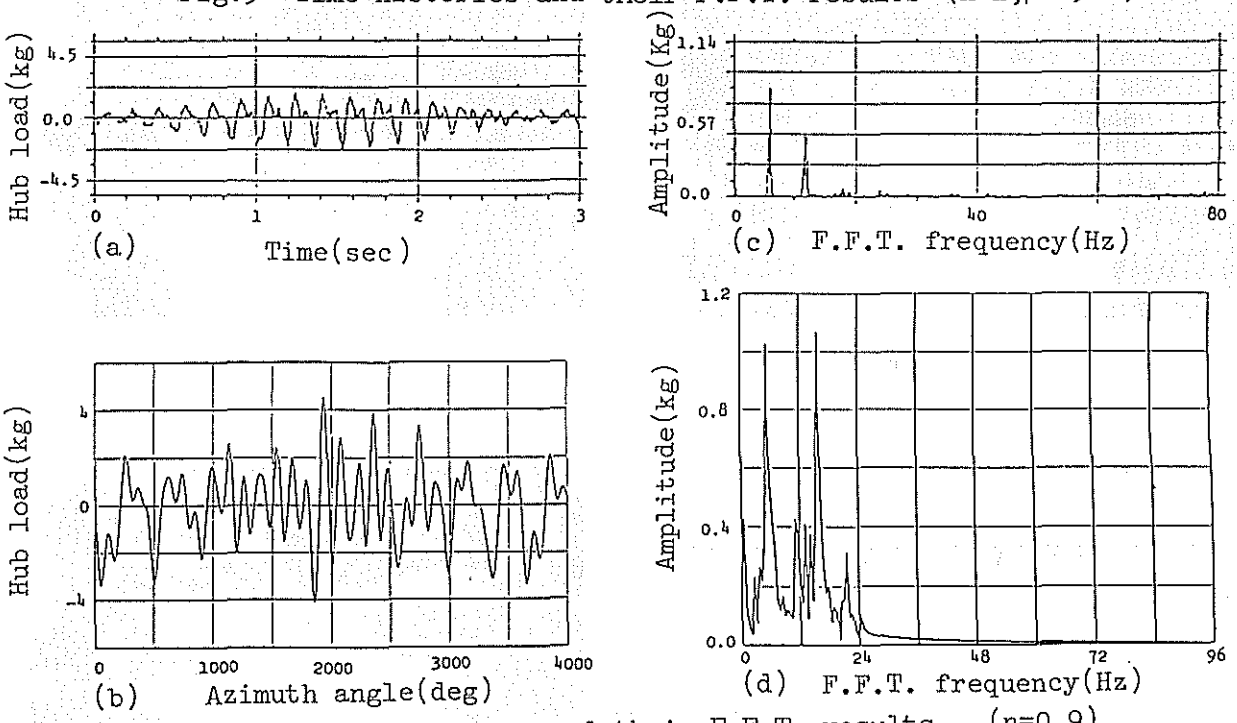

Fig.10 Time histories and their F.F.T. results (n=0.9)

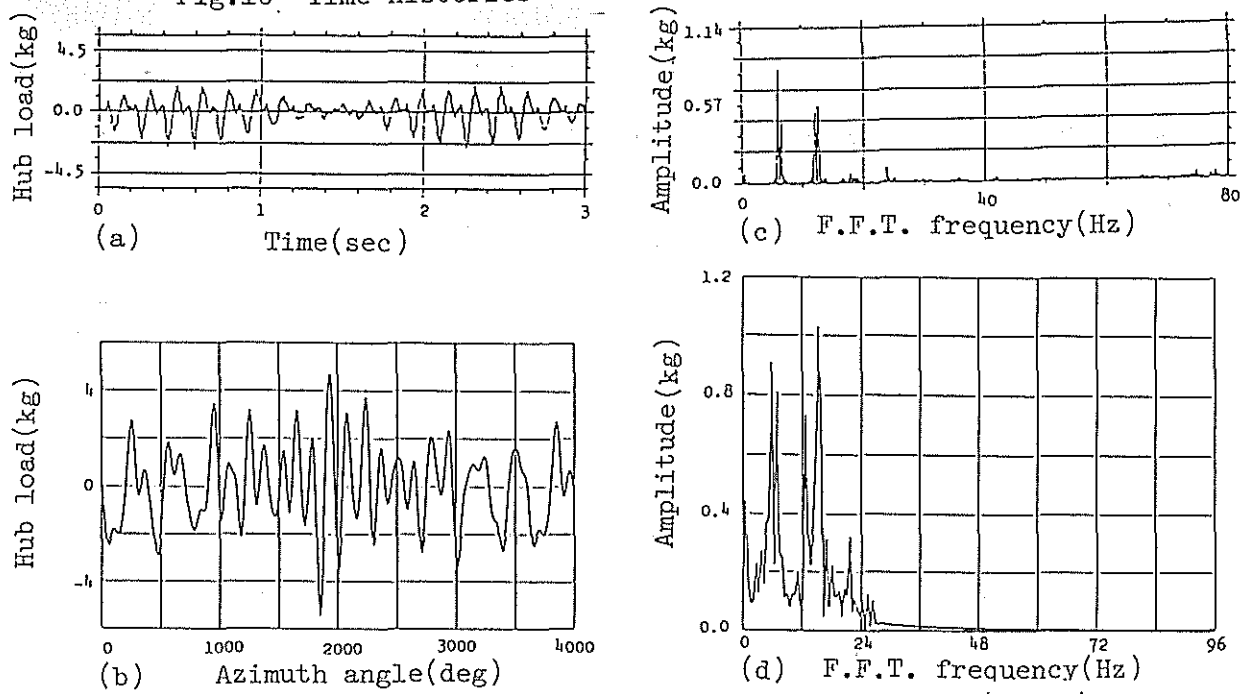

Fig.11 Time histories and their F.F.T. results (n=1.1)